Crystal Chemistry of a New Solid Solution in the $BaO-Bi_2O_3-Nb_2O_5$ System: $Ba_{5x/2}Bi_{(1-x)5/3}Nb_5O_{15}$

B. Muktha,[†] A. Simon,[‡] J. Darriet,*[,‡] and T. N. Guru Row*[,†]

Solid State and Structural Chemistry Unit, Indian Institute of Science, Bangalore 560012, India, and Institut de Chimie de la Matière Condensée de Bordeaux, CNRS, 87, Avenue A. Schweitzer, 33608 Pessac Cedex, France

Received November 3, 2005. Revised Manuscript Received December 28, 2005

A solid solution of the type $Ba_{5x/2}Bi_{(1-x)5/3}Nb_5O_{15}$ has been identified in the $BaO-Bi_2O_3-Nb_2O_5$ system for the first time. The limits of the solid solution are within the range $0.52 \leq x \leq 0.80$. The compositions $x = 0.52$, 0.60, 0.72, 0.77, 0.78, and 0.80 were synthesized by the solid-state technique from the starting materials in stoichiometric quantities. The powder X-ray patterns of all the phases in the domain indicate a structural similarity to tetragonal tungsten bronzes (TTBs). The compositions below $x = 0.52$ and those above $x = 0.80$ exhibit barium niobate and bismuth niobate impurities, respectively. Single crystals of the composition $x = 0.77$ were obtained by the melt cooling technique. The crystal structure of $Ba_{3.85/2}Bi_{1.15/3}Nb_5O_{15}$ ($x = 0.77$) was solved in the tetragonal space group *P4bm* (No. 100) with $a = 12.4938$ (14) Å, $c = 3.9519$ (2) Å, $V = 616.87$ (10) Å^3, and $Z = 2$ and was refined to an R index of 0.034. Dielectric measurements on all the phases indicate a typical relaxor behavior with a broad phase transition at $T_m \approx 300$ K.

Introduction

Bismuth-containing oxides have been extensively studied because of their interesting properties, including ferroelectricity,[1] ionic conductivity,[2] superconductivity,[3] and catalysis.[4] Since the discovery of ferroelectricity in $BaTiO_3$[5] several decades ago, the property has been a subject of interest, particularly as it relates to dielectric and structural properties of various oxides. Ferroelectric materials have applications in various technological devices, such as microwave telecommunications progress involving satellite broadcasting and random access memories in computers.[6]

Ferroelectric materials may be classified into two categories, classical ferroelectrics and relaxors, depending on their dielectric, polarization, and phase-transition behavior.[7] Classical ferroelectrics exhibit a sharp maximum in the thermal variation of the dielectric permittivity and a sharp progressive disappearance of the spontaneous polarization with an increase in temperature, which may be related to a first or a second-order phase transition. Relaxors, on the other hand, exhibit a broad maximum in the thermal variation of dielectric permittivity in addition to an increase in the temperature T_m at the maximum of the dielectric constant ($\epsilon'_{r\,max}$) and a decrease in the magnitude of the latter with increasing frequency. The development of macroscopic polarization is not observed without the application of an electric field, and the induced macropolarization disappears at a temperature well below T_m.

Among bismuth-containing ferroelectric oxides, the Aurivillius phases have been extensively studied in terms of structure and their correlation with properties. These type of oxides were first reported in 1949 by Aurivillius,[8] who described the formation of a series of layered bismuth oxides, the Aurivillius phases of the general form $[M_2O_2][A_{n-1}B_nO_{3n+1}]$, where $n = 1$, 2, 3, etc. and M is usually Bi. The A site cations could include Ca^{2+}, Sr^{2+}, Ba^{2+}, Pb^{2+}, Bi^{3+}, Na^+, rare earth ions, or mixtures of these, whereas the octahedral B site invariably contains a highly charged cation such as Ti^{4+}, Nb^{5+}, Ta^{5+}, Mo^{6+}, or W^{6+}. The structure consists of $[M_2O_2]^{2+}$ layers interwoven between the $(n-1)$ perovskite layers of composition $[A_{n-1}B_nO_{3n+1}]^{2-}$. Spontaneous polarization in these materials is ascribed to both the displacements of the B cations as well as the tilting of BO_6 octahedra. The Aurivillius type oxides exhibit a great variability in the metal-cation stoichiometry, thus presenting a potential systematic control of the physical and chemical properties. Further, these materials have been reported to have better fatigue endurance than the most widely studied bismuth oxide layered ferroelectric, $Bi_4Ti_3O_{12}$.[9] These materials also have the advantage of being lead-free, enabling various technological applications.

Relaxors of lead-based ceramics, such as $PbMg_{1/3}Nb_{2/3}O_3$ (PMN), $PbSc_{1/2}Ta_{1/2}O_3$ (PST), and $PbIn_{1/2}Nb_{1/2}O_3$ (PLZT),

* To whom correspondence should be addressed. E-mail: ssctng@sscu.iisc.ernet.in.
[†] Indian Institute of Science.
[‡] Institute de Chimie de la Matière Condensée de Bordeaux.

(1) Park, B. H.; Kang, B. S.; Bu, D. S.; Noh, T, W.; Lee, J.; Jo, W. *Nature* **1999**, *401*, 682.
(2) Boivin, J. C.; Mairesse, G. *Chem. Mater.* **1998**, *10*, 2870.
(3) Withers, R. L.; Thompson, J, G.; Wallenberg, L. R.; Fitzgerald, J. D.; Anderson, J. S.; Hyde, B. G. *J. Phys. C: Solid State Phys.* **1988**, *21*, 6067.
(4) Moro-Oka, Y.; Ueda, W. *Adv. Catal.* **1994**, *40*, 233.
(5) Wul, B.; Goldman, L. B. *C. R. Acad. Sci. URSS* **1945**, *46*, 139.
(6) Waser, R.; Rudiger, A. *Nature Mater.* **2004**, *3*, 81.
(7) Cross, E. L. *Ferroelectrics* **1994**, *151*, 305.
(8) Aurivillius, B. *Ark. Kemi* **1950**, *2*, 19.
(9) Amanuma, K.; Hase, T.; Miyasaka, Y. *Appl. Phys. Lett.* **1995**, *66*, 221.

10.1021/cm052422j CCC: $33.50
Published on Web 02/07/2006

are of great interest for applications in capacitors and actuators.[10] However, the volatility and toxicity of PbO has led to the discovery of relaxor lead-free ceramics with a perovskite structure. Solid solutions of the type $Ba(Ti_{1-x}M_x)O_3$ (M = Zr, Sn, Ce)[11] and $Ba_{1-x}K_{x/2}La_{x/2}TiO_3$ [12] have been reported to show relaxor properties. In all these materials, the relaxor effect appears when at least two different cations occupy the same crystallographic site A or M and is enhanced when the value of x is higher at the M site.[13] Another prerequisite is that at least one of the ions at the M site must be ferroelectrically active (for example Ti^{4+}, Nb^{5+}, or Ta^{5+}) in order for the cation to be off-center at the octahedral site, hence giving rise to a local dipolar moment.

The tetragonal tungsten bronzes[14] (TTBs) represent yet another large group of ferroelectric materials. $PbNb_2O_6$ was the first compound of the TTB family of oxides discovered to have a ferroelectric phase transition.[15] The tungsten bronze structure can be regarded as being a derivative of the classical perovskite ABO_3, in which the BO_3 framework is transformed to create A interstices larger than the cuboctahedron. Hence the structure can be described as a complex array of distorted octahedral sharing corners in a way that three different types of interstices A, B, and C are available for cation substitution with a general formula $(A1)_2(A2)_4C_4(B1)_2(B2)_8O_{30}$. The A1 cavities have a cuboctahedral coordination of oxygen atoms; the A2 cavities have a pentagonal prismatic coordination, and the C sites have a trigonal prismatic one. The B1 and B2 sites are substituted with octahedral coordination. The size of these cavities decreases in the order A2 > A1 > C. In a typical TTB structure, the alkali or alkaline earth metal ions occupy the A2 and A1 sites; the C site is occupied only by a small ion such as lithium, whereas the B1 and B2 sites can be substituted by tetravalent Ti or pentavalent Nb and Ta. The size and type of substituted ions on the different sites and the amount of disorder have a significant effect on the dielectric properties of these materials.

Compositions of the type $[(A1)_5(A2)_1(B1)_3(B2)_7]O_{30}$ form a typical tetragonal tungsten bronze structure. The solid-solution system strontium barium niobate $(Sr/Ba)_5Nb_{10}O_{30}$[14,16] is one of the most widely investigated systems among the TTBs. In this structure, only Ba and Sr atoms occupy five of the six A1 and A2 sites, whereas the C sites are empty. Monovalent cations can also be substituted, as in the case of $KSr_2Nb_5O_{15}$ [17] and $Ba_2NaNb_5O_{15}$.[18] Divalent alkali/alkaline earth metal ions can also be substituted by trivalent rare earth ions as $M_{6-x}^{2+}Ln_x^{3+}Nb_{10}O_{30}$.[19] In this context, several quaternary systems such as $(Sr/Ba)_5R(Ti/Nb/Ta)_7O_{30}$ [20] (R = La, Nd, Sm, Y) and $Ba_5LaTi_{3-x}Zr_xNb_7O_{30}$ [21] have been investigated for their dielectric properties.

The relaxor effect in several TTB types of compounds appears when at least two cations occupy the same crystallographic site. The coexistence of cations is favorable both at M and A sites, as in the case of perovskites. Simon et al. have reported the relaxor characteristics of TTB type lead-free relaxors containing lanthanum and bismuth.[22] However, the structural aspects of bismuth-substituted TTB relaxors are not known. In this context, we have isolated a solid solution, $Ba_{5x/2}Bi_{(1-x)5/3}Nb_5O_{15}$, in the $BaO-Bi_2O_3-Nb_2O_5$ system within the domain $0.52 \le x \le 0.80$ for the first time. Phases of compositions $Ba_{2.6/2}Bi_{2.4/3}Nb_5O_{15}$ ($x = 0.52$), $Ba_{3/2}Bi_{2/3}Nb_5O_{15}$ ($x = 0.60$), $Ba_{3.6/2}Bi_{1.4/3}Nb_5O_{15}$ ($x = 0.72$), $Ba_{3.85/2}Bi_{1.15/3}Nb_5O_{15}$ ($x = 0.77$), $Ba_{3.9/2}Bi_{1.1/3}Nb_5O_{15}$ ($x = 0.78$), and $Ba_{4/2}Bi_{1/3}Nb_5O_{15}$ ($x = 0.80$) in the domain were synthesized by the solid-state technique and characterized by powder X-ray diffraction. We also report the single-crystal X-ray structure of $Ba_{3.85/2}Bi_{1.15/3}Nb_5O_{15}$ ($x = 0.77$) and preliminary dielectric measurements on compositions $x = 0.52$, 0.72, 0.78, and 0.80.

Experimental Section

Synthesis and Crystallization. Bi_2O_3 (Fluka, 99.99%) and Nb_2O_5 (Sigma Aldrich, 99.99%) were dried at 600 °C for 4 h, and $BaCO_3$ (Fluka, 99%) was dried at 180 °C for 4 h before use. Polycrystalline samples of the phases $x = 0.52$, 0.60, 0.72, 0.77, 0.78, and 0.80 in the solid solution $Ba_{5x/2}Bi_{(1-x)5/3}Nb_5O_{15}$ were synthesized by the solid-state method using $BaCO_3$, Bi_2O_3, and Nb_2O_5 in stoichiometric quantities. The starting materials were ground well in an agate mortar and fired at 650 °C for 12 h and at 1100 °C for 12 h. The resulting mixtures were ground well and fired at 1250 °C for 24 h followed by regrinding and refiring at 1250 °C for 24 h. All the syntheses were carried out under an oxygen atmosphere. There was no weight loss observed during synthesis for any of the compositions. The progress of the reactions was monitored by powder X-ray diffraction, which confirmed the formation of a single phase in each case in the domain. DTA-TG data were obtained under a constant flow of a nitrogen atmosphere on an SDTQ 600 DTA/DSC instrument.

Single crystals of $Ba_{3.85/2}Bi_{1.15/3}Nb_5O_{15}$ ($x = 0.77$) were obtained by melting the polycrystalline sample at 1350 °C for 1 h in a platinum crucible followed by slow cooling at 1 °C h^{-1} up to 1100 °C and then slowly cooling to room temperature. A part of the obtained single crystals were ground well, and the powder pattern was recorded. The pattern obtained was similar to that of the polycrystalline sample. The selection of the single crystal was on the basis of the size and sharpness of the diffraction spots. It is noteworthy that the energy dispersive X-ray analysis (JEOL JSM-840) on the same single crystal used for the diffraction experiment gave the percentages of the Bi/Ba/Nb ions as 24.5/5.35/70, which matches the calculated atomic percentages thus providing confirmatory evidence of the composition.

Characterization. *Powder X-ray Diffraction.* Powder X-ray diffraction data of all the phases were collected at room temperature on a Philips X'Pert Pro diffractometer using Cu Kα radiation. Data

(10) Uchino, K. *Ferroelectrics* **1994**, *151*, 321.
(11) Ravez, J.; Simon, A. *Eur. Phys. J.: Appl. Phys.* **2000**, *11*, 9.
(12) Ravez, J.; Simon, A. *Mater. Lett.* **1998**, *36*, 81.
(13) Ravez, J.; Simon, A. *J. Solid State Chem.* **2001**, *162*, 260.
(14) Jamieson, P. B.; Abrahams, S. C.; Bernstein, J. L. *J. Chem. Phys.* **1968**, *48*, 5048.
(15) Goodman, G. *J. Am. Ceram. Soc.* **1953**, *36*, 368.
(16) (a) Liu, S. T.; Maciolek, R. B. *J. Electron. Mater.* **1975**, *4*, 91. (b) Fang, T.-T.; Chen, E.; Lee, W. J. *J. Eur. Ceram. Soc.* **2000**, *20*, 527.
(17) Lanfredi, S.; Cardoso, C. X.; Nobre, M. A. L. *Mater. Sci. Eng., B* **2004**, *112*, 139.
(18) Jamieson, P. B.; Abrahams, S. C.; Bernstein, J. L. *J. Chem. Phys.* **1969**, *50*, 4352.
(19) Chen, X. M.; Sun, Y. H.; Zheng, X. H. *J. Eur. Ceram. Soc.* **2003**, *23*, 1571.
(20) Singh, N. K.; Choudhary, R. N. P.; Panigrahi, A. *Mater. Lett.* **2002**, *57*, 36.
(21) Sun, Y. H.; Chen, X. M. *Mater. Res. Bull.* **2004**, *39*, 1247.
(22) Simon, A.; Ravez, J. *Phys. Status Solidi* **2003**, *3* 541.

Table 1. Crystallographic Data for $Ba_{3.85/2}Bi_{1.15/3}Nb_5O_{15}$

empirical formula	$Ba_{3.85/2}Bi_{1.15/3}Nb_5O_{15}$
cryst habit, color	parallelepiped, colorless
cryst size (mm^3)	$0.02 \times 0.02 \times 0.04$
cryst syst	tetragonal
space group	*P4bm*
a (Å)	12.4938(14)
c (Å)	3.9519(2)
V (Å^3)	616.87(10)
fw	1049
D_x (g/cm^3)	5.6460(9)
Z	2
F(000)	929
scan mode	φ-scan + ω-scan
θ_{max}	40
recording reciprocal space	$-22 \le h \le 22$, $-22 \le k \le 22$, $-6 \le l \le 6$
no. of measured reflns	26891
no. of independent reflns	1552 with $I > 3\sigma(I)$ [R(int) = 0.0443]
μ (mm^{-1})	17.301
refinement	F^2
no. of variables	68
R(F)	0.0341
wR(F^2)	0.0840
GoF	1.93
max/min dr (e/Å^3)	2.00/−2.83

were collected over the angular range $5° \le 2\theta \le 120°$ in steps of $\Delta(2\theta) = 0.008°$. The X-ray diffraction data were refined by a Le Bail profile analysis using the Jana 2000[23] program suite. The background was defined by the Chebsheyev polynomial function using 15 coefficients, and the peak shapes were described by a pseudo-Voigt function that varied five profile coefficients. For each diffraction pattern, a scale factor, a zero-error factor, shape, and unit cell parameters were refined.

Single-Crystal X-ray Diffraction. Single-crystal X-ray diffraction data were collected on a Bruker Nonius Kappa CCD diffractometer using sealed-tube Mo Kα radiation monochromated by oriented graphite. Data were reduced using specific programs of the diffractometer. An absorption correction was applied by the Gaussian method. The structure was solved by direct methods using SHELXS97[24] and refined using Jana2000. Crystallographic data and the details of the single-crystal data collection are given in Table 1. The atomic coordinates are listed in Table 2.

Ferroelectric Measurements. Dielectric measurements were performed on circular pellets of 8 mm diameter thickness that were sintered under an oxygen atmosphere at 1100 °C. Gold electrodes were deposited by dc sputtering before dielectric measurements. The diameter shrinkage $\Delta\varphi/\varphi$ was systematically determined as $(\varphi_{init} - \varphi_{fin})/\varphi_{init}$. The real ϵ'_r and imaginary ϵ''_r relative permittivities were determined on a Wayne-Kerr 6425 component analyzer under a helium flow as a function of temperature (80−600 K) and frequency (10^2 to 2×10^5 Hz). Samples were degassed under vacuum for 6 h at 600 K prior to measurements.

Results and Discussion

Crystal Structure. Single-crystal diffraction data on the $x = 0.77$ composition of the solid solution $Ba_{5x/2}Bi_{(1-x)5/3}Nb_5O_{15}$ were indexed into the tetragonal system, with $a = 12.4938$ (14) Å, $c = 3.9519$ (2) Å, $V = 616.87$ (10) Å^3, and $Z = 2$. Space group *P4bm* was assigned on the basis of the systematic absences. The positions of the Ba, Bi, and Nb atoms were obtained by direct methods. Nb(1) was located at the *2b* site and Nb(2) occupies the general position. Ba(1) occupies the 4-fold *2a* site, whereas Ba(2) lies on the mirror plane (*4c* site). Subsequent difference Fourier synthesis revealed all the remaining oxygen atoms.

During the initial stages of refinement, Ba(1) and Ba(2) were found to have large thermal parameters. This reduced considerably when Ba(1) and Bi(1) were constrained at the same site. However, the isotropic thermal parameters of Bi(1) and Ba(1) refined to an agreeable value when the coordinates of Bi(1) were refined. The refinement resulted in displacements along all three coordinates and was the highest for the *z* coordinate. Further, the occupancies of the atoms were refined in order to achieve the stoichiometry resulting in the best fit for values of 0.094 and 0.134 for Bi(1) and Ba(1), respectively. The occupancy refinement of Ba(2) resulted in a value of 0.902. Selected bond distances are given in Table 3.

A view of the structure along the *c* axis is shown in Figure 1. The crystal structure of $Ba_{3.85/2}Bi_{1.15/3}Nb_5O_{15}$ is built of two crystallographically independent NbO_6 octahedra joined via oxygen corners into a three-dimensional network. In this network, there are three types of structural channels running along the polar *c* axis. The narrowest cavities with a triangular cross section (C sites) are empty. The tetragonal cavities, A1, are occupied by the Ba(1) and Bi(1) atoms; the largest cavities, A2, with a pentagonal cross-section, are filled by Ba(2). Bi(1) has a typical one-sided coordination of oxygen atoms attributed to the projection of its $6s^2$ lone pair, whereas the one-sided coordination of Ba(1) may be ascribed to the disorder between Bi(1) and Ba(1) at the site.

The Bi(1) atom has three short bonds (2.385−2.62 Å) with $O4^a$, $O4^e$, and $O5^a$ and six long bonds (2.740−2.915 Å) with $O4^b$, $O4^c$, $O4^d$, $O4^f$, $O5^b$, and $O5^c$ thus resulting in a BiO_9 polyhedron. Ba(1) has an 8-fold coordination with four each of symmetry-related O(4) and O(5) atoms with bond distances 2.779 and 2.60 Å, respectively. Ba(2), on the other hand, is connected to six oxygen atoms, $O(1^a)$, $O(1^b)$, and four symmetry-related O(2) atoms, with bond distances of

Table 2. Final Atomic Coordinates and Equivalent Thermal Parameters (U_{eq}) at 298 K

atom	wycoff site	occupancy factor	x	y	z	U_{eq} (Å^2)[a]
Bi(1)	*8d*	0.094(1)	0.03091(14)	0.0011(15)	0.5111	0.0266(5)
Ba(1)	*2a*	0.132 (2)	0	0	0.6396(16)	0.0266(5)
Ba(2)	*4c*	0.90(1)	0.172701(18)	0.672701(18)	0.5272(7)	0.02197(8)
Nb(1)	*2b*	1	0	0.5	0.0304(8)	0.01861(14)
Nb(2)	*8d*	1	0.07275(2)	0.21109(3)	0.0281(6)	0.01730(9)
O(1)	*4c*	1	0.2157(2)	0.2843(2)	0.048(3)	0.0148(9)
O(2)	*8d*	1	−0.15616(19)	0.4937(2)	0.021(2)	0.0266(9)
O(3)	*2b*	1	0	0.5	0.519(3)	0.0410(16)
O(4)	8d	1	0.1412(3)	0.0709(3)	0.0679(19)	0.0282(12)
O(5)	8d	1	0.0763(4)	0.2054(3)	0.519(2)	0.0469(15)

[a] $U_{eq} = -(2\pi^2(U_{11}(ha^*))^2 + (U_{22}(kb^*))^2 + (U_{33}(lc^*))^2 + 2U_{12}hka^*b^* + 2U_{12}hla^*c^* + 2U_{23}klb^*c^*)$.

Table 3. Selected Bond Distances for $Ba_{3.85/2}Bi_{1.15/3}Nb_5O_{15}$

Bi(1)−O(4[a])	2.393(11)	Ba(2)−O(1[a])	2.734(9)
Bi(1)−O(4[b])	2.740(10)	Ba(2)−O(1[b])	2.850(9)
Bi(1)−O(4[c])	2.784(17)	Ba(2)−O(2) × 2	2.892(6)
Bi(1)−O(4[d])	2.915(10)	Ba(2)−O(2) × 2	2.859(6)
Bi(1)−O(4[e])	2.544(18)	Nb(2)−O(1)	2.008(3)
Bi(1)−O(4[f])	2.872(17)	Nb(2)−O(2)	1.930(3)
Bi(1)−O(5[a])	2.62(2)	Nb(2)−O(4[a])	1.956(4)
Bi(1)−O(5[b])	2.91(2)	Nb(2)−O(4[b])	2.002(4)
Bi(1)−O(5[c])	2.835(11)	Nb(2)−O(5[a])	1.942(8)
Ba(1)−O(4) × 4	2.600(8)	Nb(2)−O(5[b])	2.014(8)
Ba(1)−O(5) × 4	2.779(4)	Nb(1)−O(2) × 2	1.953(3)
		Nb(1)−O(3[a])	1.931(2)
		Nb(1)−O(3[b])	2.021(12)

2.734−2.892 Å. The coordination of oxygen atoms around Bi(1), Ba(1), and Ba(2) is shown in Figure 2. Nb(1) has symmetry-related O(2) atoms at the apexes of the octahedron, whereas the equatorial plane consists of the other two symmetry-related O(2) atoms, $O3^a$ and $O3^b$, in the range 1.931−2.021 Å. Nb(2) has O2 (1.93 Å) and $O4^a$ (1.956 Å) at the apexes of the octahedron, whereas atoms O1, $O4^b$, $O5^a$, and $O5^b$ with distances of 1.942−2.014 Å form the equatorial plane. The displacement of the Nb atoms from the center of the octahedron is characterized by the difference in the Nb−O distances to the axial and equatorial oxygen atoms that form the chain.

The $Nb(1)O_6$ octahedra are connected to $Nb(2)O_6$ octahedra via O(2), and $Nb(2)O_6$ polyhedra are linked to each other by O(4). Bi(1)/Ba(1) polyhedra in the tetragonal cavity are surrounded by eight NbO_6 octahedra with each cross-section comprising four $Nb(2)O_6$ octahedra linked via O(5).

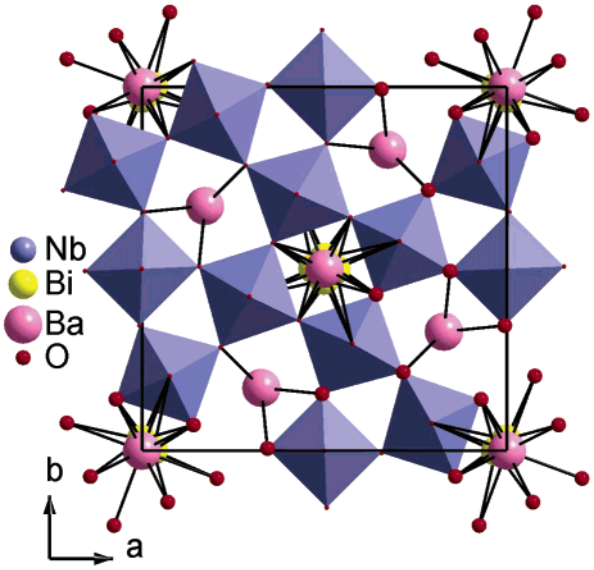

Figure 1. Crystal structure of $Ba_{3.85/2}Bi_{1.15/3}Nb_5O_{15}$ viewed along the *c* axis.

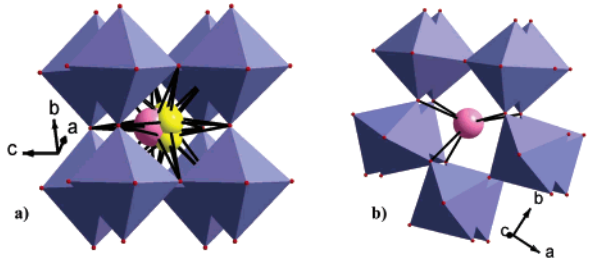

Figure 2. Coordination of (a) Ba1/Bi(1) and (b) Ba(2).

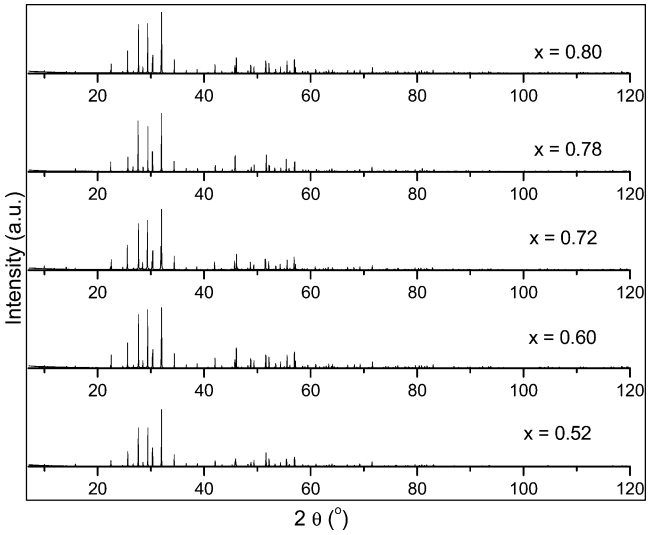

Figure 3. Powder X-ray patterns of various members of the solid solution $Ba_{5x/2}Bi_{(1-x)5/3}Nb_5O_{15}$.

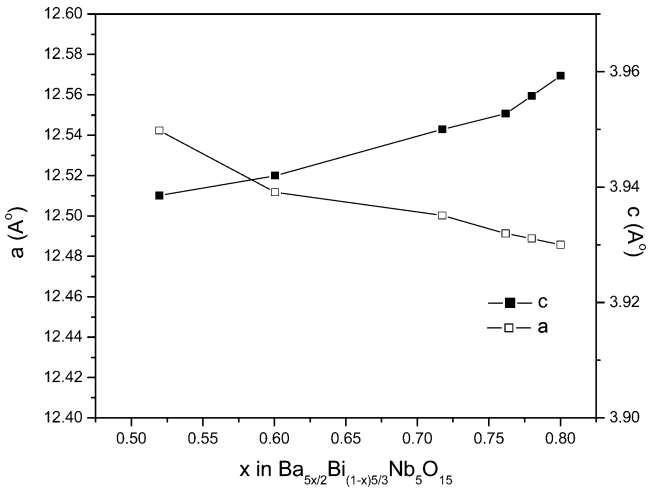

Figure 4. Evolution of cell parameters *a* and *c* with composition.

The empty triangular cross-section is surrounded by one $Nb(1)O_6$ octahedron and two $Nb(2)O_6$ octahedra. The Ba(2) atom at the pentagonal cavity is surrounded by 10 NbO_6 octahedra. The pentagonal cross-section comprises one $Nb(1)O_6$ octahedron and four $Nb(2)O_6$ octahedra.

The powder X-ray patterns of the compositions 0.52, 0.60, 0.72, 0.78, and 0.80 in the solid solution $Ba_{5x/2}Bi_{(1-x)5/3}Nb_5O_{15}$ are shown in Figure 3. The lattice parameters obtained from the single-crystal X-ray data for the composition $x = 0.77$ were used to fit the profile for each powder pattern. The evolution of unit cell parameters *a* and *c* for $x = 0.52$, 0.60, 0.72, 0.78, and 0.80 in the solid solution $Ba_{5x/2}Bi_{(1-x)5/3}Nb_5O_{15}$ is shown in Figure 4. The unit cell parameter *a* decreases with an increase in the composition of barium. The *c* parameter shows an increasing trend with an increase in the composition of *x*. Thus, the *a* and *c* parameters show a gradual increase and decrease in values, respectively, with an increase in the barium content.

(23) Petricek, V.; Dusek, M. *Jana 2000, Structure Determination Software Programs*; Institute of Physics: Praha, Czech Republic, 2000.
(24) Sheldrick, G. M. *SHELXL97, Program for Crystal Structure Refinement*; University of Göttingen: Göttingen, Germany. 1997.

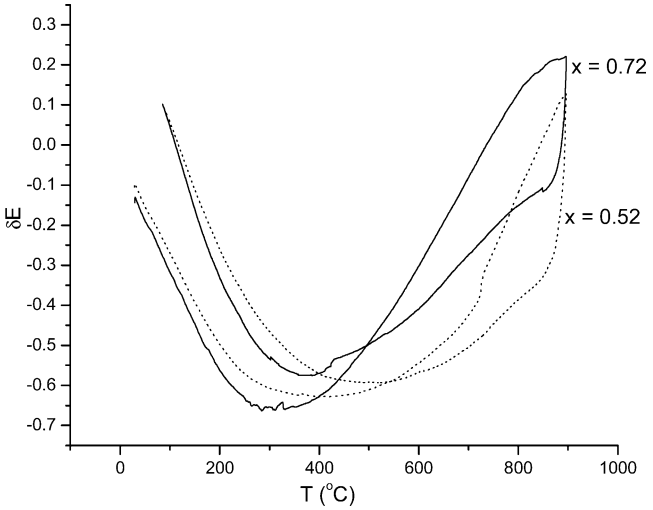

Figure 5. DTA plots of $x = 0.52$ and 0.72 in $Ba_{5x/2}Bi_{(1-x)5/3}Nb_5O_{15}$.

Compositions $x = 0.10$, 0.20, 0.30, 0.40, 0.45, 0.85, and 0.90 were synthesized from their stoichiometries to check the formation of any solid solution within a different range. The X-ray powder patterns of compositions $x > 0.80$ and $x < 0.52$ show the presence of the $BaNb_2O_6$ (minor) phase along with the TTB (major) phase. Prolonged heating of compositions $x = 0.10$, 0.20, 0.30, 0.40, and 0.45 at 1250 °C resulted in melting of the phases. It is to be noted that there was no change observed in the powder patterns for all these compositions even after melting. The compositions $x = 0.85$ and 0.90 did not melt at 1250 °C; however, the impurity peaks remained even after prolonged heating at 1250 °C. This clearly establishes the lower and upper limits of the solid solutions at $x = 0.52$ and $x = 0.80$, respectively.

DTA-TG data were recorded in the range 150−900 °C for the TTB compositions $x = 0.52$ and 0.72 in the solid solution $Ba_{5x/2}Bi_{(1-x)5/3}Nb_5O_{15}$, as shown in Figure 5. The plots indicate a broad irreversible phase transition without any weight loss throughout the range. The broad endothermic phase transition may be indicative of composition fluctuation attributable to the disorder of cations at the bismuth and barium sites.

Dielectric Measurements. Dielectric measurements indicate typical relaxor behavior for compositions $x = 0.52$, 0.72, 0.78, and 0.80 in the solid solution $Ba_{5x/2}Bi_{(1-x)5/3}Nb_5O_{15}$. A very broad peak appears in the range 100−600 K and shifts to the low-temperature side with decreasing frequency. Such a diffused dielectric anomaly is the typical characteristic of relaxors.[25] Also, a high-temperature dispersive anomaly was found ($T > 500$K) for all the compositions. In connection with the strong and continuous dispersion of both ϵ'_r and ϵ''_r, this high-temperature anomaly can be ascribed to a

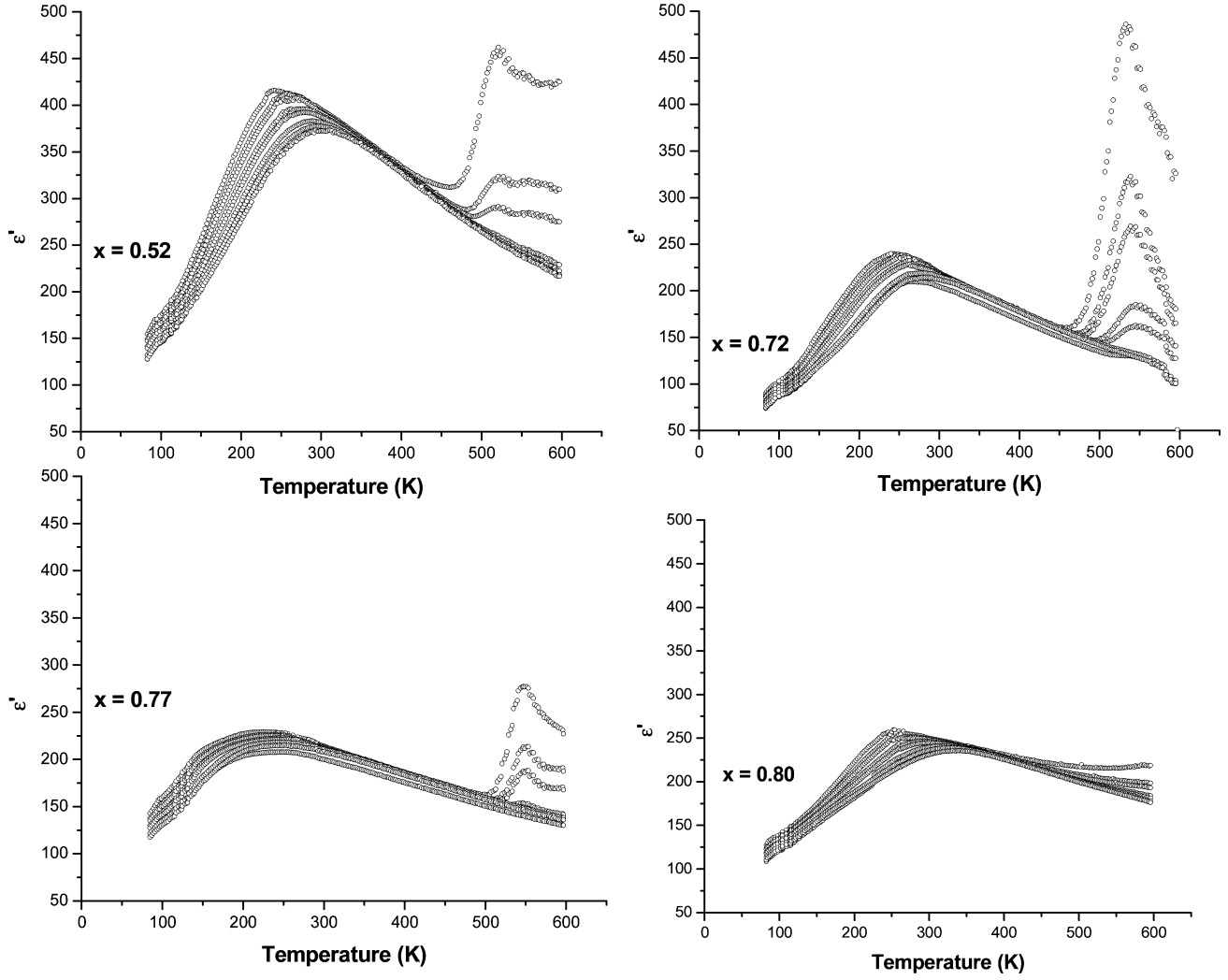

Figure 6. Thermal variation of the real part of permittivity, ϵ'_r, for $x = 0.52$, 0.72, 0.77, and 0.80 in the solid solution $Ba_{5x/2}Bi_{(1-x)5/3}Nb_5O_{15}$.

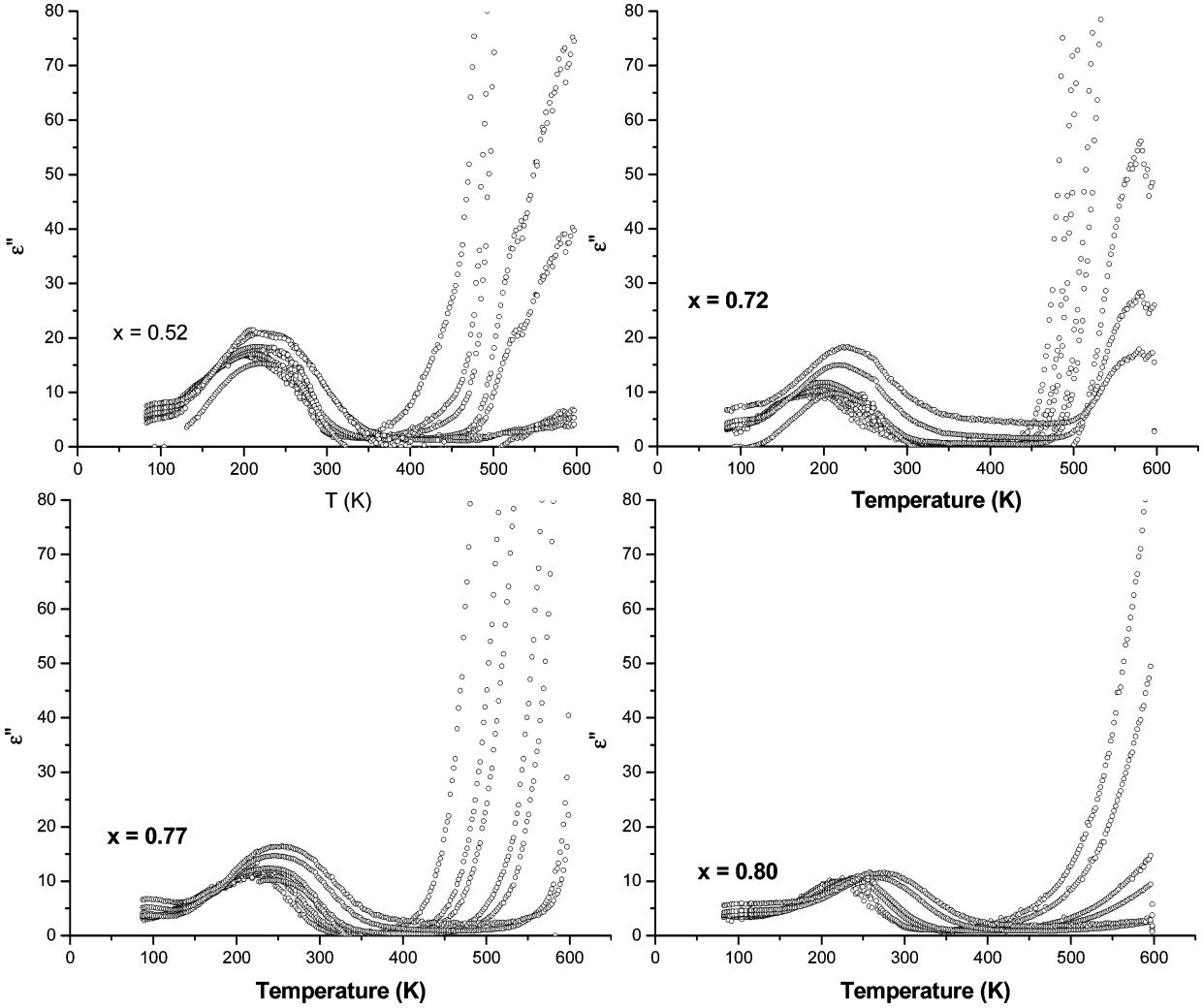

Figure 7. Thermal variation of the imaginary part of permittivity, ϵ''_r, for $x = 0.52$, 0.72, 0.77, and 0.80.

conductivity-related relaxation. The conductivity could be due to the oxygen ions that can hop through the interlinked $Nb(2)O_6$ octahedra. An observation of the conductivity-related frequency dispersion curves indicates a decrease in conductivity as the higher limit of the solid solution $x = 0.80$ approaches.

The thermal evolution of ϵ'_r, the real part of the dielectric permittivity, shows a broad maximum at T_m that is shifted to higher temperatures with an increase in frequency (Figure 6). On the other hand, the maximum value ϵ'_r max decreases. A shift is observed in the temperature T_m of the maximum of the imaginary part of the dielectric permittivity ϵ''_r to higher values as the frequency increases (Figure 7); but contrary to the evolution of ϵ'_r, the evolution of the frequency dispersion here is characterized by an increase in ϵ''_r when the frequency is increased. Because of compositional disorder between Bi(1) and Ba(1) atoms, the compositions studied show relaxor behavior even below room temperature. It is to be noted that the values of dielectric permittivity ϵ'_r are much lower compared to those of CBN[26] ($Ca_xBa_{1-x}Nb_2O_6$) and SBN[25] ($Sr_{1-x}Ba_xNb_2O_6$) types of relaxors with a TTB structure.

Summary

A solid solution of the form $Ba_{5x/2}Bi_{(1-x)5/3}Nb_5O_{15}$ has been evidenced for the first time in the $BaO-Bi_2O_3-Nb_2O_5$ system in the range $0.52 \leq x \leq 0.80$. The structural type of the compositions in the system is similar to that of tetragonal tungsten bronzes. The crystal structure of one of its members, $x = 0.77$, depicts a one-sided coordination for Ba(1) because of the disorder between Ba(1) and Bi(1). Also, the disorder in the occupancies of the Bi(1) and Ba(1) atoms gives rise to a typical relaxor behavior in these materials. DTA curves indicate a very broad exothermic phase transition, indicating a fluctuation in composition that occurs very slowly. High-temperature powder X-ray diffraction studies are in progress. Preliminary dielectric measurements indicate a very broad peak that is typical of relaxor materials. Further, dielectric constants for the compositions studied in the solid solution show lower values compared to those of other TTB systems despite the presence of Bi, which has a stereochemically active $6s^2$ lone pair. The compositions also show reasonably good conductivity as observed from the dispersion at the

(25) Cross, L. E. *Ferroelectrics* **1987**, *76*, 241.
(26) Qi, Y. J.; Lu, C. J.; Zhu, J.; Chen, B.; Song, H. L.; Zhang, H. J.; Xu, X. G. *Appl. Phy. Lett.* **2005**, *87*, 082904.

high-temperature regime, which may be attributed to oxygen migration through the interlinked NbO_6 octahedra.

Acknowledgment. B.M. thanks CSIR, India, for a senior research fellowship and LAFICS (IFLACS) for financial assistance. We acknowledge Dr. M. Maglione, ICMCB, for helpful discussions on the dielectric measurements.

Supporting Information Available: CIF files for the crystals. This material is available free of charge via the Internet at http://pubs.acs.org. This information has also been deposited at the Fachinformationzentrum Karlsruhe (FIZ) with the number CSD 415840.

CM052422J